

Collapse Risks of Fail-Safe RC Frames Due to Earthquakes: Fragility Assessments

Sindur P. Mangkoesoebroto^{1,2}, Made H. Prayoga^{1,2} & Rizkita Parithusta²

¹Civil Engineering Department, Faculty of Civil and Environmental Engineering, Institut Teknologi Bandung, Jalan Ganesha 10, Bandung 40132, Indonesia ²Indonesia Center for Earthquake Engineering, Jalan Dr. Curie 21, Bandung 40171, Indonesia *E-mail: sindurpm@gmail.com

Abstract. The objective of this study was to determine the collapse risk of failsafe reinforced concrete (RC) frames due to earthquakes by newly developed fragility curves. The curves were constructed based on the collapse mechanism, instead of measures of lateral drift as customarily adopted. The procedure was applied to RC open frames that were seismic resistant. A fail-safe mechanism was imposed by allowing plastic hinges to be formed mainly in the beams. This automatically satisfied the stronger column-weaker beam requirement; shear failure was neither tolerated anywhere in the columns nor in the beams. Two kinds of fail-safe RC frames were investigated: special moment resisting frames (SMF) and ordinary moment resisting frames (OMF). Their earthquake collapse risk was computed and compared. Inelastic time history (NLTH) and the nonlinear static procedure (NSP) were conducted to assess their structural performance. The results showed among others that the fail-safe OMF had lower collapse risk than the fail-safe SMF. The collapse prevention performance level in NLTH could only be achieved for the fail-safe frames. The non-linear time history analysis should be the only method used for seismic reevaluation/safety checking of building frame structures.

Keywords: collapse risk; earthquake; fail-safe reinforced concrete frame; fragility; NSP; time history.

1 Introduction

The research reported in this paper was motivated, in part by the destructive earthquakes that hit Indonesia in the last decade, such as Aceh (2004, $M_{\rm w}=9.1$), Padang (2007, $M_{\rm w}=8.4$), Java (2009, $M_{\rm w}=7.0$), Lombok (2018, $M_{\rm w}=6.9$), and Sulawesi (2018, $M_{\rm w}=7.5$) (USGS [1]). The earthquakes caused heavy damage to humans and structures both engineered and non-engineered. This raised questions, especially regarding the engineered structures, whether their design and construction were executed properly, or some other measures need to be taken. As regulated, all engineered structures have to be designed and constructed in accordance with the Indonesian National Standard (abbreviated as SNI) codes [2-4]. Further, special moment frame concrete

Received November 2nd, 2018, 1st Revision January 28th, 2019, 2nd Revision March 6th, 2019, Accepted for publication July 25th, 2019.

Copyright ©2019 Published by ITB Journal Publisher, ISSN: 2337-5779, DOI: 10.5614/j.eng.technol.sci.2019.51.4.3

building structures are required to be detailed following fully ductile section rules to prevent premature failure during major earthquakes.

The study was applied to the model of a reinforced concrete open building frame as detailed in Section 2. The structure was located at coordinates 6°53′16″S, 107°36′27″E, as part of the PSTNT Batan (Nuclear Research Reactor) Bandung building compound. The frame belongs to the Design Class 3 of IAEA [5] and accordingly should be designed following conventional building codes with particular attention to stability and structural integrity. Based on the seismic study for this particular site detailed in Section 3, the structure needed to be designed and constructed following the most stringent criteria based on the concrete and seismic SNIs [3,4]. This was facilitated by the development of the fail-safe design methodology investigated in this study, which is discussed in Section 4.2, emphasizing the collapse risk. The collapse risk was determined as the convolution integral of the seismic fragility of the structure and the site-specific hazard relation (Section 5).

The concept of fragility of structures, systems and components was developed initially in the nuclear community (Kennedy, *et al.* [6]). However, its widespread use in structural engineering, especially in the past decade, has been acknowledged; an extensive literature review can be found in Elnashai, *et al.* [7]. Recently, Nazri, *et al.* [8] developed fragility curves for regular and irregular concrete and steel frames, and concluded that irregular frames exhibit a higher probability of reaching operational phase and collapse prevention levels than regular ones. Ibrahim, *et al.* [9] employed fragility curves to assess the seismic damage of multi-story structures and one of their conclusions was that the structural performance of the different structural models was not very dissimilar.

Hosseinpour, et al. [10] generated fragility curves for RC frames under a series of earthquakes. Among the findings was that the fragility curves were highly affected by the earthquake region and therefore earthquake characteristics should be thoroughly evaluated before deriving the fragility curves. Al Mamun, et al. [11] developed seismic fragility curves of reinforced concrete buildings in Canada designed after 1985 and assessed the vulnerability of the buildings due to earthquakes. Differences between two parts of the country were markedly observed. Moon, et al. [12] employed a fragility approach to investigate the effect of plan structural irregularity and confirmed that the more irregular the structures, the higher the risk they pose. Meanwhile, the effect of the soil-structure interaction on the fragility curves was investigated by Anvarsamarin, et al. [13] with the finding that adopting the average spectral acceleration (S_{a.avg}) intensity measure is more efficient in capturing the effect of the inherent uncertainties of strong ground motions on the structural response parameters.

Thus far the construction of the fragility curves was based on the attainment of some measures of lateral drift against the PGA [7] or its variants. In some cases, the ensemble of the ground motions employed was not fully matched to a specific target spectrum, making them contain wide variability. The variability of the quantities involved was then combined to yield the aelatory uncertainty, β_R . Consequently, the collapse mechanism of the structure was not properly reflected in β_R . In this study the generation of the fragility curves was directly related to the collapse mechanism of the structure at a given PGA.

In the study, the lognormal fragility curves were generated based on an alternative method as proposed in Section 4. The method is deemed to be more suitable for seismic resistant frames designed by load-and-resistant factor design (LRFD) as well as allowable stress design (ASD). The safety factor in ASD, denoted by FS, was employed to lower the nominal value of the yield strength to the nominal design level; the load factors were unity. The FS was associated with the structure reliability index, β_C , in LRFD. The minimum value of β_C was associated with the load combination involving seismic load as an extreme event.

A collapse criterion associated with a fail-safe collapse mechanism in the frame's critical direction was considered in this study. The mechanism was thus used to avoid collapse by the story mechanism commonly associated with excessive plastic hinge formation at the columns at intermediate levels. The computed total story drift and/or the maximum inter-story drift ratio were also discussed and compared.

2 The Fail-Safe Model Frames

The concepts developed in this paper were elaborated via a building frame model commonly found in practice, as shown in Figure 1. It is constructed of reinforced concrete material of 35 MPa compressive strength for the beams, and 40 MPa for the columns (with steel rebar of 400 MPa tensile strength), eightstory (4 m for the lowest story plus seven @ 3.5 m), four-bay (6 m) in one direction, and six-bay (5 m) in the perpendicular direction. The structure was strictly designed based on the Indonesian SNIs [2-4].

Two classes of designs were executed for two frames with identical dimensions, one a special moment resisting frame (SMF), and the other an ordinary moment resisting frame (OMF); they only differed in the amount of steel reinforcement. However, both satisfied the fail-safe criterion as they were seismically resistant.

The fail-safe criterion was associated with the fail-safe collapse mechanism illustrated in Figure 6, allowing no premature failure prior to flexural beam sectional plastification. Shear failure was neither tolerated in the beams nor in the columns and plastification was allowed only in a few columns. Consequently, for the special moment frame (SMF), the shear strength was designed based on the probable beam-end section flexural strength in addition to all applicable gravity loads. The stronger column-weaker beam criterion as ruled by a factor of 6/5 in SNI [3] was satisfied and even increased for the structure to perform safely at higher performance levels (LS and CP). The confinement requirements for SMF were also satisfied at the beams and the columns. For OMF the fail-safe criterion allowed no premature failure due to shear. More than the shear design based on SNI [3], the fail-safe shear design was based on the beam-end flexural capacity in addition to all applicable gravity loads. Lack of column-to-beam moment capacity ratio was not tolerated. To further clarify this concept, the fail-safe and code models are defined in Section 4.1.

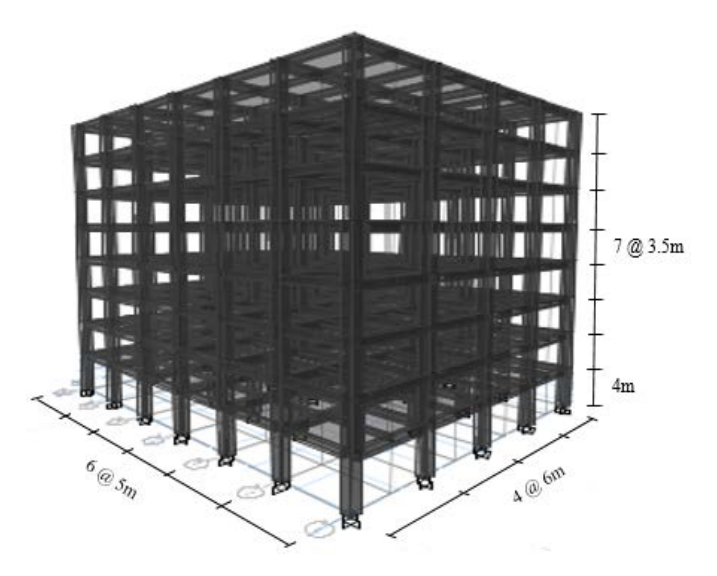


Figure 1 Open frame model of eight-story building. Lowest story 4 meters and seven stories @ 3.5 meters; four spans @ 6 meters, six @ 5 meters perpendicular. Fundamental period $T_1 = 1.31$ seconds. Fixed bases.

The minimum loads as stipulated in SNI [2] were applied. The live load was 2.5 kN/m² for the slabs, 1 kN/m² for the roofs, a superimposed dead load of 0.9 kN/m² for the slabs and 0.6 kN/m² for the roofs. The mass associated with these loads gave rise to a structural fundamental period of $T_1 = 1.31$ seconds, slightly lower than the maximum required by SNI [4] of 1.33 seconds. The importance

factor was $I_e = 1$, and the response modification factors R = 8 (SMF) and R = 3(OMF). The seismic load was applied through a site-specific response spectrum design for mean-plus-sigma (84-percentile). The typical beam and column reinforcements are shown in Tables 1 and 2. Due to the requirements of base shear scaling and minimum reinforcement ratio, the main reinforcements of SMF and OMF were the same, except for the beam sections at the supports. The beam shear reinforcement for the OMF was performed by the fail-safe model (Section 4.2).

| | | Support | | | | Midspan | | | |
|----------|--------|---------|-------------|------|-------------|---------|--------------|------|--------------|
| Beam | | SMF | | OMF | | SMF | | OMF | |
| | | Main | Shear | Main | Shear* | Main | Shear | Main | Shear |
| B350x700 | Top | 5D16 | 2D10- 90 | 7D16 | 2D10- 90 | 5D16 | 2D10- 150 | 5D16 | 2D10- 150 |
| | Bottom | 5D16 | | 5D16 | | 5D16 | | 5D16 | |
| B300x600 | Top | 3D16 | 2D10- 90 | 5D16 | 2D10- 90 | 3D16 | 2D10- 200 | 3D16 | 2D10- 200 |
| | Bottom | 3D16 | | 4D16 | | 3D16 | | 3D16 | |
| B350x600 | Top | 4D16 | 2D10- 90 | 6D16 | 2D10- 90 | 4D16 | 2D10- 160 | 4D16 | 2D10- 160 |
| | Bottom | 4D16 | | 4D16 | | 4D16 | | 4D16 | |
| B300x500 | Top | 3D16 | 2D10- 90 | 4D16 | 2D10- 90 | 3D16 | 2D10- 200 | 3D16 | 2D10- 200 |
| | Bottom | 3D16 | | 3D16 | | 3D16 | | 3D16 | |

Table 1 Typical beam reinforcements (all units in mm).

Table 2 Typical column reinforcements (all units in mm).

| G-1 | S | MF | OMF | | | |
|----------|-------|---------|-------|---------|--|--|
| Column | Main | Shear | Main | Shear* | | |
| C700x700 | 28D16 | 8D10-90 | 28D16 | 8D10-90 | | |
| C600x600 | 20D16 | 6D10-80 | 20D16 | 6D10-80 | | |
| | | | | | | |

^{*} Designed by the fail-safe OMF (Section 4.2).

The structure was detailed in such a way that it could develop stable plastic hinges at the beam ends. In the computation, the plastic hinges were modeled by a moment-curvature relation (M-φ) that was validated by the experiment reported in Mangkoesoebroto, et al. [14]. The IO, LS, and CP performance levels in the M-φ relation were defined based on FEMA [15], see Table 4.

3 **Seismic Hazard and Ground Motion Analyses**

The seismic parameters presented in this section are the updated summary of a full seismic study carried out by Mangkoesobroto, et al. [16] for the specific site in question. Both the probabilistic (PSHA) and the deterministic (DSHA) approaches were performed to yield mean-plus-sigma (84-percentile) as well as median (50-percentile) values. The former was used in the design of the frame stipulated by SNI [4] as described in Section 2, while the latter was employed in evaluating the collapse risk in accordance with IAEA [5] (Section 5). The 84-percentile acceleration target spectrum considering both PSHA and DSHA is shown in Figure 2, while the hazard curves in Figure 3. Figure 4 are plots of the hazard curves, H(a) versus the PGA, a, for median values considering both PSHA and DSHA.

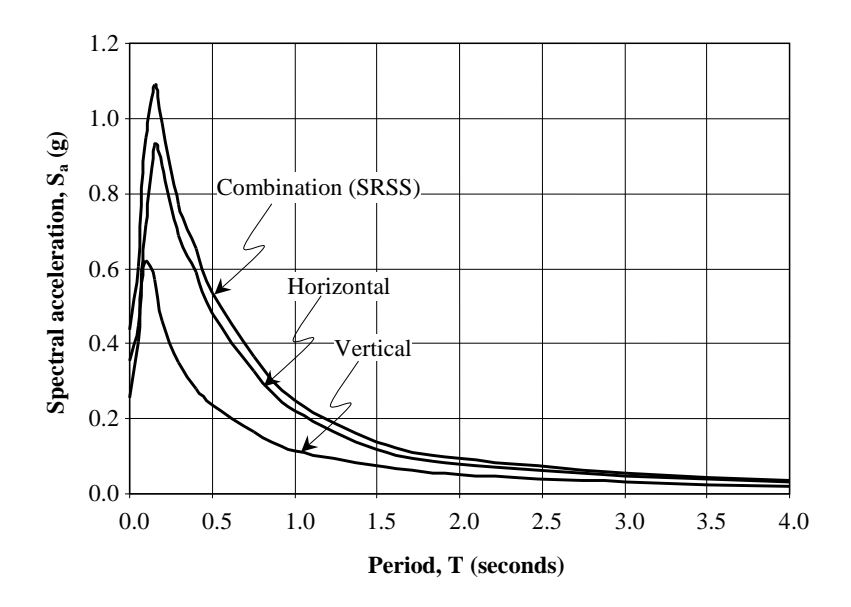


Figure 2 The design spectral acceleration (mean-plus-sigma). Maximum credible earthquake peak ground acceleration is 0.44 g (SRSS).

The controlling earthquake source for the site is the Lembang fault, located at northern side of the site. The fault has the property of a normal focal mechanism, with a seismogenic distance of $r_{\rm seis}=17.5$ km, magnitude $M_{\rm w}=6.7$, and depth H=33 km. The shear wave velocity of the rock at the site was measured to be $V_{\rm s}=1,050$ m/sec. The resulting maximum credible earthquake (MCE) is 0.35 g (H) and 0.26 g (V); the square-root-of-the-sum-of-the-squares (SRSS) combination is 0.44 g (84-percentile) – see the response spectrum in Figure 2.

The 84-percentile hazard curve (Figure 3) shows that an MCE of 0.44 g corresponds to an earthquake with a return period of about $T_R = 3,500$ years, which was employed in the design process of the building frame, together with the response spectrum in Figure 2. Meanwhile, the hazard curve of the median values (MCE_M = 0.29 g) was necessary for computing the collapse risk [5] and to perform the spectral matching of the three-component ground motions.

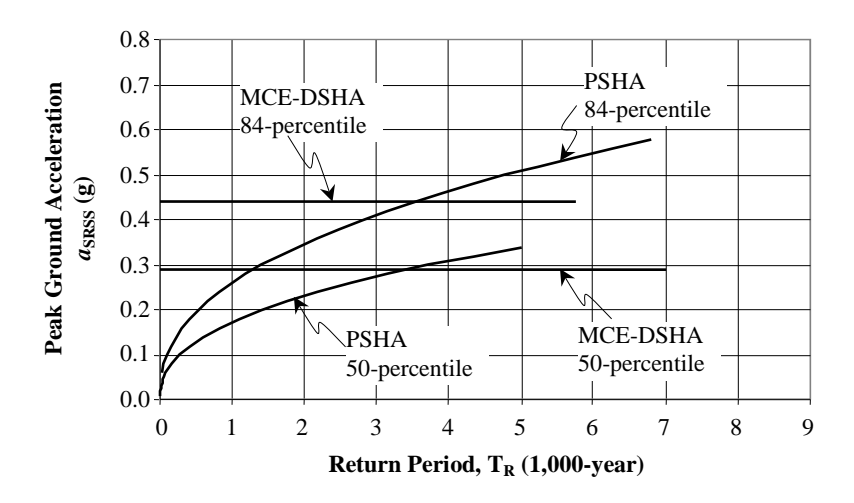


Figure 3 The probabilistic and deterministic seismic hazard curves for 50- and 84-percentiles. SRSS combination of horizontal and vertical components.

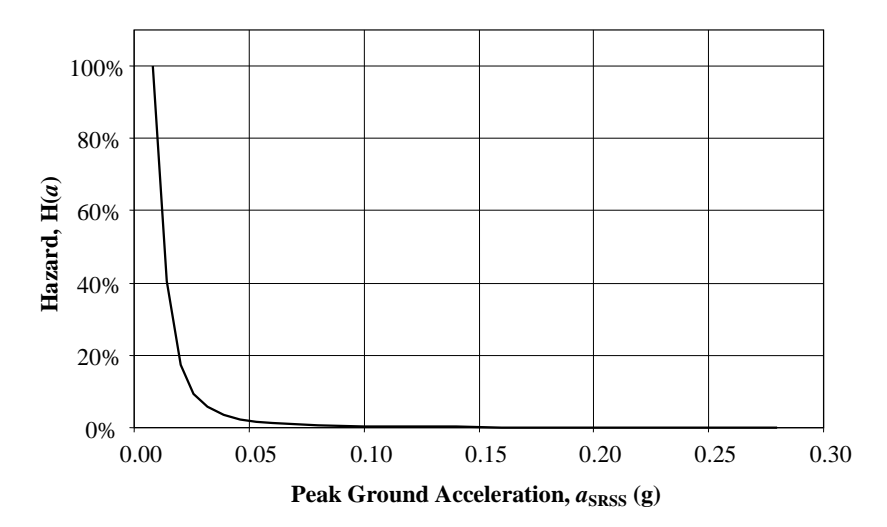


Figure 4 Median value site-specific hazard curve considering PSHA and DSHA. Median value of the maximum credible earthquake is $MCE_M = 0.29$ g.

The ground motion data shown in Table 3 were downloaded from PEER [17]. The peak ground acceleration (PGA) is in the range of 0.27-0.69 g, and the peak ground velocity (PGV) is in the range of 22-80 cm/sec, both in the major direction. The acceleration time series were all spectrally matched to the median target spectrum for all frequencies and for all three components, but the ratio between the minor PGA and that of a major was retained. Consequently, all earthquake data have the same spectral response as shown in Figure 2.

The matched acceleration records were then applied to excite the RC frame model shown in Figure 1 in a non-linear time history (NLTH) analysis. It was expected that the structure would progress through IO, LS, and finally the CP performance levels complying with the fail-safe criterion set in Section 2. If it did not, then a strengthening step was performed to satisfy the fail-safe, e.g. increasing the main column rebars and consequently the shear reinforcement to avoid excessive column hinges. This process was necessary for the construction of the fragility curves.

| | | | | | - | | | | | | |
|---------------------------------|---------------------------|---------------|-------|--------|------|-------|--------|------|------------|--------|------|
| | | | Major | | | Minor | | | Vertical | | |
| Earthquake event | $\mathbf{M}_{\mathbf{w}}$ | Depth (km) | PGA | PGV | PGD | PGA | PGV | PGD | PGA | PGV | PGD |
| | | (MII) | (g) | (cm/s) | (cm) | (g) | (cm/s) | (cm) | (g) | (cm/s) | (cm) |
| El Mayor- | | | | | | | | | | | |
| Cucapah (2010) | 72 | 15 | 0.54 | 62 | 35 | 0.41 | 44 | 21 | 0.80 | 17 | 8.6 |
| Erzican Turkey (1992) | 6.7 | 20 | 050 | 78 | 28 | 0.39 | 107 | 32 | 0.23 | 16 | 10 |
| Imperial Valley-07 (1979) | 65 | 12 | 0.27 | 26 | 5.4 | 0.16 | 15 | 5.4 | 0.08 | 15 | 5.4 |
| Imperial Valley-06 (1979) | 65 | 12 | 0.28 | 22 | 10 | 0.20 | 19 | 16 | 0.19 | 7 | 2.7 |
| Kobe Japan (1995) | 6.9 | 18 | 033 | 45 | 28 | 0.28 | 34 | 27 | 0.34 | 28 | 7.4 |
| Mammoth Lakes-02 (1980) | 6.0 | 7 | 0.44 | 24 | 3.6 | 0.39 | 24 | 3.7 | 0.26 | 9 | 15 |
| N. Palm Springs (1986) | 6.0 | 10 | 0.69 | 66 | 16 | 0.67 | 28 | 4.9 | 0.38 | 12 | 15 |
| Parkfield (1966) | 62 | 9 | 036 | 22 | 5.6 | 0.27 | 15 | 3.1 | 0.14 | 45 | 15 |

Table 3 Employed earthquake data and their properties.

4 The Structural Fragility

The conditional probability of occurrence of a specific performance level at a given peak ground acceleration, a, or fragility $P_{\text{IIIA}}(a)$, is generally assumed to be lognormal. The lognormal fragility employed herein, expressed in Eq. (1), with PGA as the independent variable [6], has found wide applicability in structural engineering [7],

$$P_{|||A}(a) = \Phi\left(\frac{\ell n \binom{a/a_M} + \beta_U \Phi^{-1}(Q)}{\beta_R}\right)$$
 (1)

where Φ is the normal cumulative distribution function; a, a_M are the peak ground acceleration and its median values; β_U , β_R are the epistemic and aleatory uncertainties, and Q is the confidence level of the associated curve. For median value Q=50% the second term vanishes. The fragility curve is constructed by initially establishing two points on the curve for each performance level. The first point is associated with a high probability of occurrence (95% or higher), while the second is associated with a low one (5% or lower).

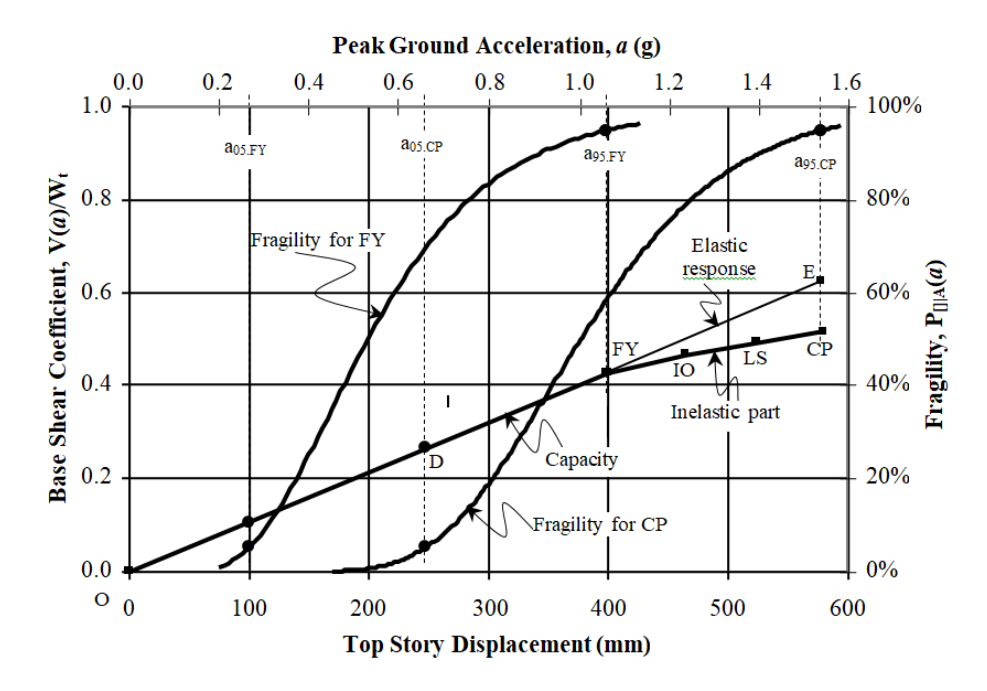


Figure 5 The capacity curve is superimposed with the median fragility curves. The FY fragility is for linear elastic part (O-FY); the CP for inelastic (O-FY-CP). Line O-E represents the elastic response.

The fragility curves were developed for FY, IO, LS, and CP performance levels. The structure was excited by three-component ground motions in the time history analysis; in total eight ground motions for eight computer runs were set. The CP level was associated with a high collapse risk, e.g. 95-percentile or higher. The collapse was defined such that all CP potential beam plastic hinges

were formed in the frame; in this case, in the weak direction while subjected to the major component of the seismic ground motion. The PGA was increased gradually until ninety-five percent of the total CP beam plastic hinges were noticed. The fail-safe criterion was then checked. When 95% of the CP beam plastic hinges were formed at a certain PGA value, this value is denoted by $a_{95.CP}$, i.e. associated with 95% collapse risk. Thus there are eight values of $a_{95.CP}$ for the eight sets of ground motions and the median value was documented. The next step was to determine the second $a_{05.CP}$ point, associated with a low collapse risk. This was elaborated with reference to Figure 5.

Figure 5 illustrates the capacity curve (base shear coefficient $V(a)/W_t$ versus rooftop displacement) superimposed on its fragilities, i.e. conditional probability P_{IIIA} versus PGA. Point D is supposed to be the design point. A structure that is designed properly can perform elastically without cracking up to this point. When the load is further increased the structure starts having to mobilize its safety factor (SF) up to the first yield point, FY. The safety factor is defined as the base shear at FY divided by the base shear at point D. Moreover, if the structure is properly detailed, much further response can reach point CP by mobilizing its collapse prevention ductility factor, μ_{CP} . At this CP point, 95% or more CP beam plastic hinges have developed. The collapse prevention ductility factor is defined as the displacement at CP divided by that at FY.

The safety factor (SF) can be related to the capacity reliability index, β_C . For lognormally distributed random variables the following expression can be readily derived for small coefficients of variation:

$$SF = \frac{C_n}{Q_n} = \frac{\lambda_C \hat{\mu}_C}{D_n + L_n + E_n} \approx \frac{\lambda_C \hat{\mu}_Q \exp\left[\beta_C \sqrt{V_C^2 + V_Q^2}\right]}{\lambda_D \hat{\mu}_D + \lambda_L \hat{\mu}_L + \lambda_E \hat{\mu}_E}$$
(2)

where SF is the safety factor, C_n is the structure's nominal capacity, Q_n is the nominal load effect, e.g. dead (D_n) plus live (L_n) plus earthquake (E_n) nominal load effects, or $Q_n = D_n + L_n + E_n$; the λ 's are the bias factors, i.e. the ratio between the nominal and the mean values, generally close to unity; $\hat{\mu}$, V are the mean values and the coefficients of variation, respectively; $\beta_C(a_D) = \Phi^{-1}[1-P_{CP|A}(a_D)]$ is the capacity reliability index. Upon rearrangement, Eq. (2) can be written as,

$$SF = \frac{\lambda_{C}}{\lambda_{E}} - \frac{\frac{\hat{\mu}_{D}}{\hat{\mu}_{E}} + \frac{\hat{\mu}_{L}}{\hat{\mu}_{E}} + 1}{\frac{\lambda_{D}}{\lambda_{E}} \frac{\hat{\mu}_{D}}{\hat{\mu}_{E}} + \frac{\lambda_{L}}{\lambda_{E}} \frac{\hat{\mu}_{L}}{\hat{\mu}_{E}} + 1} - \exp\left[\Phi^{-1}\left[1 - P_{CP|A}(a_{D})\right]\sqrt{V_{C}^{2} + V_{Q}^{2}}\right]$$
(3)

where
$$V_Q = V_E = \frac{\sqrt{\left(\frac{V_D}{V_E}\frac{\hat{\mu}_D}{\hat{\mu}_E}\right)^2 + \left(\frac{V_L}{V_E}\frac{\hat{\mu}_L}{\hat{\mu}_E}\right)^2 + 1}}{\frac{\hat{\mu}_D}{\hat{\mu}_E} + \frac{\hat{\mu}_L}{\hat{\mu}_E} + 1}$$
 (4)

The fragility of $P_{CP|A}(a_D) = 5\%$ was adopted in this study and the following mean independent parameters were used: $V_E = 0.5$, $V_D = 0.1$, $V_C = 0.11$, $V_L = 0.2$, $\lambda_E = 1.0$, $\lambda_D = 1.05$, $\lambda_C = 0.95$, $\lambda_L = 1.0$, $\hat{\mu}_D/\hat{\mu}_E = 0.4$, $\hat{\mu}_L/\hat{\mu}_E = 0.2$. Most of these values are listed in Ellingwood, *et al.* [18]. A sensitivity analysis was performed by varying $\pm 10\%$ of one parameter from its mean value while holding the others fixed, which showed that the most sensitive parameters were λ_C , λ_E , V_E , respectively. The least sensitive parameters were V_D , V_L , $\hat{\mu}_L/\hat{\mu}_E$, V_C , respectively. The remaining ones were moderately sensitive. The resulting safety factor was SF = 1.51-1.73 (ninety-percentile confidence level) with mean value $\hat{\mu}_{SF} = 1.62$. Fragility $P_{CP|A}(a_D) = 5\%$ in case of an extreme seismic event means that the PGA associated with point D, a_D , corresponds to a collapse risk of 5% at this given a_D . Further, $a_{05.CP} = a_D$ was determined by dividing $a_{95.CP}$ by both the collapse prevention ductility factor, μ_{CP} , and the safety factor, or $a_{05.CP} = a_{95.CP}/(\mu_{CP} \times \hat{\mu}_{SF})$, in case of an elastic design associated with point E, $a_{05.E} = a_{95.E}/\hat{\mu}_{SF}$, since the collapse prevention ductility factor was unity, $\mu_E = 1$.

The first yield (FY) level is anchored to the formation of 50% of the total FY beam plastic hinges at a certain PGA value. At this PGA value, it was assumed that a high probability (95% or higher) of 50% of FY beam plastic hinges were observed; this PGA value is denoted by $a_{95.FY}$. At lower than this PGA value $a_{95.FY}$, the structure's response is elastic linear, as shown in Figure 5. For this linear part it is expected that a seismic load of about half of $a_{95.FY}$ gives the median probability of the first yield (FY) occurring. Consequently, the median PGA value, $a_{M.FY}$, is about half of that of the ninety-five-percentile of the first yield, or more exactly $a_{M.FY} = 10a_{95.FY}/19$. Operating Eq. 1 for $a_{95.FY}$ and then for $a_{05.FY}$, and performing simple algebra, one gets $a_{M.FY} = \sqrt{a_{05.FY}.a_{95.FY}}$. Since $a_{M.FY} = 10a_{95.FY}/19$, then $a_{05.FY} = 0.277a_{95.FY}$. Moreover, the aleatory uncertainty for the linear elastic part becomes $\beta_{R.FY} = 0.39$ (for the first yield level), close to 0.37 reported in Kennedy, *et al.* [6] (for a safe shutdown earthquake).

The points IO and LS, defined in line with FEMA [15] (Table 4), were anchored in this study to 65- and 85-percent formation of all IO and LS beam plastic hinges, respectively. The PGA associated with a high probability of formation of 65% of IO beam plastic hinges is denoted by $a_{95.IO}$; $a_{95.LS}$ is defined similarly. These values of $a_{95.IO}$ and $a_{95.LS}$ were established based on computer runs in the

time history analysis, and their median values were accounted for. The low probability PGAs of the IO and LS performance levels, i.e. $a_{05.IO}$ and $a_{05.LS}$, were determined by linear interpolation of $a_{05.FY}$ and $a_{05.CP}$, respectively. Referring to Figure 5, a simple linear interpolation function is expressible as follows [19]:

$$a_{05.[]} = \frac{a_{95.CP}}{3.61 \,\mu_{CP} \,(\mu_{CP} - 1)SF} \left[\left(3.61 - SF \right) \mu_{CP} \, \frac{a_{95.[]}}{a_{95.CP}} + \mu_{CP} \, SF - 3.61 \right]$$
 (5)

where the index $_{[]}$ is substituted for IO and LS, $\mu_{CP} = a_{95,CP}/a_{95,FY} > 1$ is the collapse prevention ductility factor, $SF = \hat{\mu}_{SF} = 1.62$ is the safety factor. The median value is $a_{M,[]} = \sqrt{a_{05,[]}.a_{95,[]}}$, and the aleatory uncertainty is $\beta_{R,[]} = [\ell n(a_{95,[]}/a_{05,[]})]/3.29$. This completes the procedure of constructing the fragility curves for the FY, IO, LS, and CP performance levels. The steps of constructing the fragility curves are provided in the Appendix.

Table 4 Acceptance criteria for deformation-controlled assemblies used in nonlinear procedures for some performance levels.

| Performance Level | Drift limits FEMA [15] | Probability of plastic hinge ≥ associated performance level |
|-------------------|---------------------------|---|
| FY | - | 50% |
| IO | 50% (or less) | 65% |
| LS | 75% | 85% |
| СР | 100% | 95% |

4.1 Fragility of Special Moment Frame

Computer runs were executed to produce the response of the special moment frame (SMF) model structure in non-linear time history analysis (NLTH). The frame was subjected to earthquake loads simultaneously with full dead and part of the live loads. The earthquake records employed were the ones that had been matched to the target spectra (see Section 3). The aim was to obtain the structural response associated with the CP performance level, i.e. one that corresponds to the formation of 95% of CP beam plastic hinges satisfying the fail-safe criterion. This process was performed by iteration and the resulting PGA associated with the CP was produced. This was repeated for all the earthquake records to establish the median value, herein denoted by $a_{95 \, \text{CP}}$. The same procedure was performed for the FY, IO, and LS performance levels to obtain a_{95,FY}, a_{95,IO}, a_{95,LS}, respectively. Further, the PGA associated with 5% fragility was determined by the method described above to get a_{05,FY}, a_{05,IO}, $a_{05,LS}$, and $a_{05,CP}$. In this way the response as well as the lognormal fragility curves for the FY, IO, LS, and CP performance levels was constructed. It was found, however, that the model structure as designed strictly based on the SNIs [2-4] could only withstand a PGA value associated with the IO level. Therefore, a step to strengthen the columns was performed in order to satisfy the fail-safe criterion and to reach higher levels of performance, i.e. LS and CP. The former is referred to as the code model, while the latter is referred to as the fail-safe model. Figure 6 shows the fail-safe collapse mechanism at performance level CP of a typical fail-safe model interior frame at the end of the earthquake in NLTH.

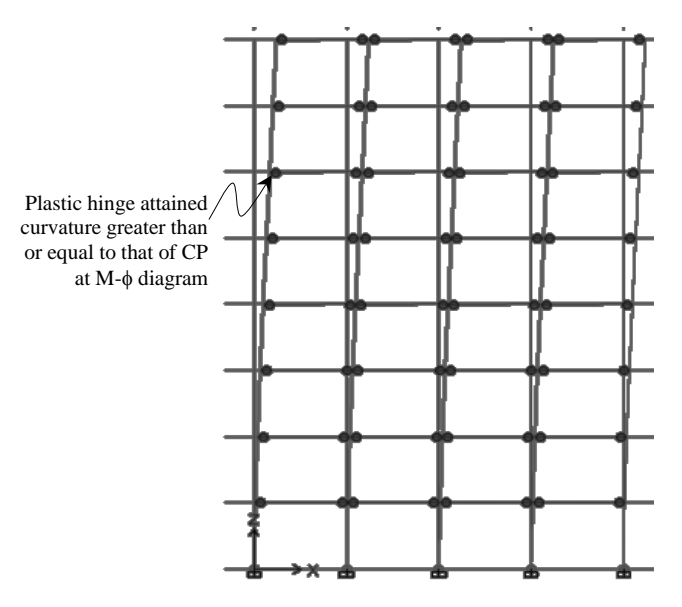


Figure 6 The fail-safe collapse mechanism of a fail-safe model interior frame (typical) at CP performance level or 95% of total CP plastic hinge formation (NLTH).

Another computer run was performed for an increasing monotonically lateral load applied to the frame models. The lateral load, distributed over all stories to simulate the earthquake, was applied gradually to get the capacity curve, spanning the elastic and inelastic regimes. The inertial force was neglected as it is a quasi-static problem. The seismic demand was determined in accordance with ATC [20], Mangkoesoebroto [21] together with the capacity curve to determine the so-called performance point (PP). This procedure is known as the non-linear static procedure (NSP). PP indicates the demand of the design earthquake and associated with this point is a PGA that corresponds to a 95% probability of achieving the PP performance level; this PGA is denoted by a_{95.PP}. The performance point ductility factor, μ_{PP} , was also determined for PP. The PGA associated with a 5% probability of achieving PP could be determined as $a_{05,PP} = a_{95,PP} / (\mu_{PP} \times SF)$. The fragility curve for PP could then be constructed. This was performed for both the fail-safe and the code model frames.

Figure 7 presents the results for two methods (NLTH and NSP), two frame models (code and fail-safe), and for the capacity as well as the fragility curves for the special moment frame (SMF). The shear reinforcement and confinement were detailed for fully ductile sections. It could be observed that the NSP yielded two curves that almost fully coincided for the fail-safe and the code model. The two models were identical in dimensions, and therefore in their fundamental periods, but differed in the amount of steel reinforcement in the columns, being stronger for the fail-safe model, to avoid excessive plastic hinges at the column sections.

Peak Ground Acceleration, a_{SRSS} (g) $0.00 \quad 0.25 \quad 0.50 \quad 0.75 \quad 1.00 \quad 1.25 \quad 1.50 \quad 1.75 \quad 2.00 \quad 2.25 \quad 2.50$ 100% 1.00 Base Shear Coefficient, $V(a)/W_1$ 0.90 90% 0.80 80% Ю F 0.70 70% 0.60 60% **FRAGILITIES** 0.50 50% **CAPACITIES** 0.40 40% NLTH – FM CP LS 30% 0.30 Ю NSP – FM 0.20 20% 0.10 10% NSP 0.00 0% 100 350 0 50 150 200 250 300 400 450 **Top Story Displacement (mm)**

Figure 7 The capacity superimposed on the median fragility curves for code (CM) and fail-safe models (FM) of special moment frames. Both for non-linear time history (NLTH) and static procedure (NSP) analyses.

NLTH was applied to the fail-safe model only, since the code model produced excessive column plastic hinges and thus could not meet the fail-safe criterion. The fail-safe model could satisfactorily pass through all performance levels, i.e. IO, LS, CP. The discrepancy between NLTH and NSP in Figure 7 is due to inertial effects. It was observed that the PP of NSP was associated with the IO in NLTH. Indeed, the PP should have been associated with the CP as both points refer to their own demand. Because of this, the NSP may not be suitable for use in seismic re-evaluation/safety checking of frame structures. As far as the displacement is concerned, the maximum top story displacement of 384 mm at CP was associated with a total story drift of 1.35%, or a maximum inter-story drift of 2%, less than the limit set in SEAOC [22] and PEER[23], 2.5% and 3%, respectively.

The fragility curves are shown in Figure 7 for the FY, IO, LS, and CP performance levels. The high and low fragility values can readily be associated with the ones in the capacity curves, e.g. $a_{95:[]}$ and $a_{05:[]}$, where the index $_{[]}$ has to be substituted for FY, IO, LS, and CP. Particularly interesting are the fragility curves for IO and PP. Though they were associated to each other, the PP fragility curve was shifted to the right side of that of IO at lower fragility values. This falsely gave better assessment of the PP level than that of IO in terms of collapse risk.

4.2 Fragility of Ordinary Moment Frame

The same procedure as with the special moment frame (SMF) model was performed with the ordinary moment frame (OMF). Two versions, the code and the fail-safe models, were investigated. The code model was basically established by designing the structure strictly based on the SNI [3] and on the fail-safe one strengthening steps were imposed to satisfy the fail-safe criterion. These included, among others, redesigning the shear reinforcement. In the fail-safe model, the shear reinforcement was designed based on the following expression:

$$V_{u,\{\}} = f(q_u, P_u) + \frac{M_{1,\{\}} + M_{2,\{\}}}{\ell} \le \phi_V V_n$$
 (6)

where
$$M_{1,\{\}} = M_{y1,\{\}} + \frac{M_{pr1,\{\}} - M_{y1,\{\}}}{\mu_{CP,SMF} - 1} (\mu_{CP,\{\}} - 1), 1 \le \mu_{CP,\{\}} \le \mu_{CP,SMF}$$
 (7)

The moment $M_{2.\{\}}$ is determined in the same way. $V_{u.\{\}}$ is the required shear strength, V_n is the nominal shear strength, ϕ_V is the shear resistance factor, $M_{y1.\{\}}$ is the section yield moment at end 1, $M_{pr1.\{\}}$ is the section probable moment at end 1, $f(q_u,P_u)$ is a function of the factored distributed and concentrated loads for uniformly distributed and moving concentrated factored loads $f(q_u,P_u)=0.5$ q_u $\ell+P_u$; ℓ is the clear span, index $_{\{\}}$ is to be substituted for OMF, SMF, or IMF (intermediate moment frame), $\mu_{CP.SMF}=R/SF=8/1.6=5$, $\mu_{CP.OMF}=R/SF=3/1.6=1.875$. Eq. (6) guaranteed that a premature shear failure prior to the mobilization of $M_{1.OMF}$ and $M_{2.OMF}$ associated with $\mu_{CP.OMF}$ would not occur. The confinement requirement was also proportionally configured.

Figure 8 shows that the code model could only survive up to point Rp at about base shear coefficient and top story displacement values $V/W_t = 0.13$ and 118 mm, respectively; the failure was brittle due to the lack of shear strength. The code model was then improved by applying Eqs. (6) and (7) for increasing the shear capacity, getting a closer spacing for better confinement and more column

rebar to avoid excessive plastification, producing the fail-safe model. Further analyses were performed to the fail-safe model. The maximum top story displacement of 282 mm at CP was associated with a total story drift of 1%, or a maximum inter-story drift of 1.6%, i.e. less than the limit set in SEAOC [22] and PEER [23], respectively. The NSP capacity curve was lower than that of NLTH as in SMF; the deviation was due to the inertial effect. The NSP performance point was associated with IO in NLTH, as in the case of SMF.

The fragility curves presented are each associated with the performance level indicated by the capacity curves. It was interesting to observe that the PGA that would cause 95% of PP (NSP) was associated with only 67% probability of causing CP (NLTH). Again, this shows the shortcomings of NSP to predict the collapse state of the structure for the associated demand. In the case of SMF (Section 4.1), this figure was around 95% of PP for 70% of CP, in close agreement with that of the fail-safe OMF.

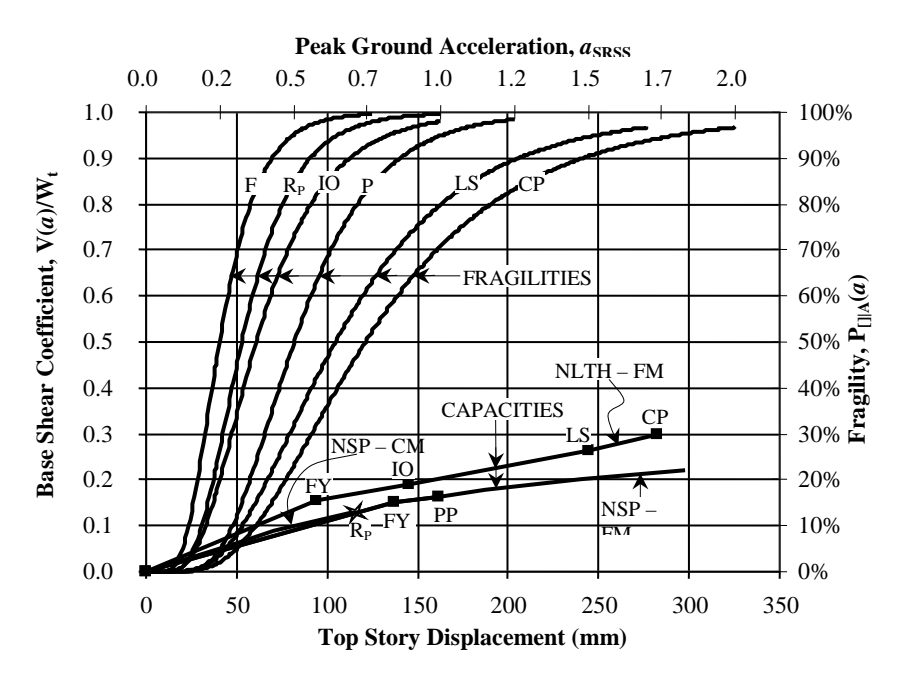


Figure 8 The capacity superimposed on the median fragility curves for code (CM) and fail-safe models (FM) of ordinary moment frames. Both for non-linear time history (NLTH) and static procedure (NSP) analyses.

5 Collapse Risk

Fragility is a conditional probability of occurrence of a specific performance level at a given peak ground acceleration, a. Meanwhile, the PGA, a, itself has

its own probability of occurrence dictated by the hazard relation, which is basically the probability of occurrence of a certain PGA level, a, in one year. Therefore, the total probability of occurrence of a specific performance level is the convolution of its conditional probability or fragility with the hazard of a for all possible a's. When the performance level in question is the structural collapse state, then the collapse risk is generally referred to. In general, it is expressible as follows [5]:

$$P_{\square} = \int_{0}^{\infty} H(a) \frac{dP_{\square|A}(a)}{da} da$$
 (8)

where index Π is to be substituted by the performance level in question, e.g. CP, LS, IO, PP, FY. The PGA hazard relation, H(a), is presented in Figure 4. Eq. (8) for P_[] is evaluated for median values; the result for CP, P_{CP}, should be smaller than the performance goal, $P_{G,CP}$. The median value of the performance goal is stipulated in SNI [4] $P_{G,CP} = 2 \times 10^{-4}$ per annum. The discrete form of Eq. (8) is as follows:

$$P_{[]} = \Delta P_{[]|A} \sum_{i} H(a_{i})$$
 (9)

Eq. (9) is employed to estimate the probability of achieving a specific performance level associated with the fragility curves constructed in Section 4. The results are tabulated in Table 5 for the frame models satisfying the fail-safe criterion, i.e. the fail-safe model computed by NLTH. It can be inferred from Table 5 that the fail-safe OMF structure poses less seismic collapse risk than the SMF; both satisfy the code's required performance goal. The former was expected since the OMF was designed for a lower collapse prevention ductility factor than that of the SMF, while both satisfy the fail-safe criterion. The positive thing is that the OMF needed lower detailing requirements than the SMF, easing the steel reinforcement issues.

Table 5 Probability of achieving a specific performance level per annum (NLTH).

| Doufournous I such | Fail-Safe Model | | | | |
|--------------------|-----------------|----------|--|--|--|
| Performance Level | SMF | OMF | | | |
| FY | 14.48E-04 | 6.12E-04 | | | |
| IO | 4.00E-04 | 2.16E-04 | | | |
| LS | 1.34E-04 | 0.38E-04 | | | |
| CP | 0.94E-04 | 0.22E-04 | | | |

Note: the performance goal for CP, $P_{G,CP} = 2 \times 10^{-4}$ per annum [4].

6 Summary and Conclusions

6.1 Summary

Code model frames were designed strictly based on SNIs [2-4], i.e. a special resisting moment frame (SMF) and an ordinary resisting moment frame (OMF). Their dimensions were identical, therefore their fundamental periods were unchanged. However, the OMF (R = 3) had more steel reinforcement than the SMF (R = 8). Two kinds of analyses were applied to the frames: non-linear time history (NLTH) and the non-linear static procedure (NSP). The frames were excited by ground accelerations in NLTH and laterally distributed static force to simulate earthquake loads in NSP, the distribution of which was associated with the first mode of the structure. In the former, the frames were excited up to the collapse prevention state (CP). The collapse should conform to the fail-safe criterion. When the frames did not perform as specified, a number of strengthening steps were carried out. These included the addition of column rebar to minimize column plastification and to increase the beam shear strength as well as confinement in accordance with the collapse prevention ductility factor being assigned to the frames. The resulting frames are referred to as failsafe models. The fail-safe models satisfied the fail-safe criterion as explained in Section 2. The consequence of adding more column rebar, both main and transverse, yielded a column-to-beam plastic moment capacity ratio about 3.5, higher than that required by SNI [3] of 6/5. However, this is in agreement with Haselton, et al. [24].

Capacity curves were constructed for the two models (Section 4). The NSP gave lower capacity curves than NLTH. The difference was due to the inertial effect, which is not accounted for in NSP. The code model SMF performed safely, as expected, up to points beyond the performance point (PP) under NSP. As predicted, the code model OMF failed in a brittle manner around its yield point due to lack of shear strength. In NLTH, two code model frames could not satisfy the fail-safe criterion and therefore they were strengthened to become fail-safe models. The fail-safe models performed safely up to collapse prevention (CP) state. Comparing the capacity curves for NSP to those of NLTH revealed that the performance point (PP) of NSP was associated with IO in NLTH. Since PP is a measure of its demand, as CP, the correspondence should be between PP and CP. A large difference between the two was observed, indicating the shortcomings of NSP. It is therefore recommended to employ NLTH for seismic re-evaluation/safety checking of frame structures.

Fragility curves were constructed in association with the capacity curve for all performance levels, i.e. FY, IO, LS, CP, and PP; for SMF and OMF, for fail-safe and code models. Constructing the fragility curves was done by initially

determining two points on the curve and then joining them by a median value lognormal distribution function according to the details given in Section 4. The fragility curves were then convoluted with a hazard function to obtain the probability of achieving a specific performance level (Table 5), e.g. collapse prevention (CP). These were performed for the fail-safe model frames analyzed by NLTH. From Table 5 it can be observed that, while both satisfied the SNI's target collapse risk, the fail-safe OMF generally showed lower risks than the fail-safe SMF. This was expected since the OMF was designed for a lower collapse prevention ductility factor than the SMF.

It is worth noting that the fail-safe SMF structure was different from the failsafe OMF in most respects. Although, lower-risk fail-safe models could be achieved by increasing the importance factor, they are still at the same level of detailing. Meanwhile, the fail-safe OMF possesses a lower level of detailing, normally taken to ease construction issues. Thus, both models meet the fail-safe criterion but with different levels of detailing. In light of this new finding, the use of fail-safe OMF structures should be allowed in all seismic regions, which thus far has been prohibited by SNI [4].

6.2 **Conclusions**

The conclusions that can be drawn are:

- 1. A new approach of constructing fragility curves based on the collapse mechanism was formulated.
- The collapse risks of the fail-safe reinforced concrete ordinary moment resisting frames were lower than those of the fail-safe special moment resisting frames.
- 3. The collapse prevention performance level could not be achieved safely except by the fail-safe frames.
- 4. Non-linear time history analysis should be the only method used for seismic re-evaluation/safety checking of building frames.
- 5. The ratio of the column-to-beam moment capacity was higher for the failsafe concrete frames than that required by the building code.
- To ease construction issues associated with the detailing, the use of fail-safe reinforced concrete ordinary moment resisting frames should be allowed in all seismic regions.

Acknowledgements

The first author acknowledges the support of the Engineering Center for Industry and the Center for Infrastructures and Built Environment, both of the Institut Teknologi Bandung. The reviewers' comments and suggestions are gratefully acknowledged.

Appendix

The following are the steps executed to construct the fragility curves developed in the paper.

- **Step 1.** Collapse definition. The collapse mechanism was defined such that 95% of all CP beam potential plastic hinges (CP level at the M-φ relations) were formed in the critical direction of the structure and only a few plastic hinges were allowed in the columns.
- **Step 2.** Time history analysis. Conduct a non-linear time history analysis for a set of three-orthogonal earthquake acceleration loads until a collapse mechanism is observed. The PGA associated with this state is denoted by $a_{95,CP}$. The index 95 is for a 95% collapse risk, which is associated with the fragility value $P_{CP|A}(a=a_{95,CP})$, while index CP shows that the fragility curve to be generated is for the CP performance level.
- **Step 3.** Repeat Step 2 for other sets of three-orthogonal earthquake accelerations, thereby producing median values of $a_{95,CP}$ and $P_{CP|A}(a=a_{95,CP})$. In this way, one point on the median fragility curve is obtained; the point is for $P_{CP|A}(a=a_{95,CP})=0.95$.
- **Step 4.** The first yield point. The PGA associated with the first yield was anchored to cause 50% formation of all FY potential plastic hinges to be equal to or exceed their yield points (FY) at the M- ϕ relations. Therefore, repeat Step 3 to obtain $a_{95,FY}$, which is the median PGA associated with the first yield point with high certainty (95% or higher).
- **Step 5.** Determination of the second point on the fragility curve. From Steps 3 and 4, the collapse prevention ductility factor μ_{CP} can be computed as $\mu_{CP} = a_{95,CP}/a_{95,FY}$. Then the PGA associated with the 5% fragility for the CP performance level is $a_{05,CP} = a_{95,CP}/(\mu_{CP} \text{ x SF})$. Note that SF = 1.62 is derived for 5% fragility, or $P_{CP|A}(a = a_{05,CP} = a_D) = 5\%$. In this way, the second point on the median fragility curve is obtained; the point is for $P_{CP|A}(a = a_{05,CP}) = 0.05$.
- **Step 6.** Determination of the median PGA and the aleatory uncertainty. The median PGA is computed as $a_{M.CP} = \sqrt{a_{05.CP}.a_{95.CP}} = a_{95.CP}/\sqrt{R}$, and the aleatory uncertainty is obtainable as $\beta_{R.CP} = [\ell n(a_{95.CP}/a_{05.CP})] / 3.29 = [\ell n(R)] /$
- 3.29, where the values of $a_{95,CP}$ and $a_{05,CP}$ are obtained in Steps 3 and 5, and $R = \mu_{CP} x$ SF is the response modification factor. Having found both, Eq. (1) is established to generate the median fragility curve of the CP performance level. The epistemic uncertainty $\beta_{U,CP}$ has no effect since only the median value is used in this study and thus $\Phi^{-1}(Q = 50\%) = 0$.
- **Step 7.** The fragility curve for the first yield (FY). The construction of the curve is elaborated in Section 4.

certainty (95% or higher); thereby the points of $P_{IO|A}(a = a_{95,IO}) = 0.95$ and $P_{LS|A}(a = a_{95,LS}) = 0.95$ are determined.

Step 9. The second points of IO and LS performance levels. The values of $a_{05.IO}$ and $a_{05.LS}$ are determined by Eq. (5). These values are associated with 5% fragilities and thereby $P_{IO|A}(a=a_{05.IO})=P_{LS|A}(a=a_{05.LS})=0.05$ are obtained.

Step 10. The median fragility curves for IO and LS. Redo Step 6 to establish the median fragility curves for IO and LS.

References

- [1] U.S. Geological Survey, *USGS Earthquake Catalog 2004-2019*, accessed from https://earthquake.usgs.gov/earthquakes/, (October 2018).
- [2] The National Standardization Agency of Indonesia (BSN), SNI 1727:2013 *Minimum Design Loads for Buildings and Other Structures*, 2013. (Text in Indonesian).
- [3] The National Standardization Agency of Indonesia (BSN), SNI 2847:2013 *Building Code Requirements for Structural Concrete*, 2013. (Text in Indonesian).
- [4] The National Standardization Agency of Indonesia (BSN), SNI 1726:2012 Seismic Provisions for Buildings and other Structures, 2012. (Text in Indonesian).
- [5] IAEA, Safety reports series No. 41: Safety of New and Existing Research Reactor Facilities in Relation to External Events, International Atomic Energy Agency, 2005.
- [6] Kennedy, R.P. & Ravindra, M.K., Seismic Fragilities for Nuclear Power Plant Risk Studies, Nuclear Engineering and Design, 79, pp. 47-68, 1984.
- [7] Elnashai, A.S. & Di Sarno, L., *Fundamentals of Earthquake Engineering:* From Source to Fragility, 2nd Ed., John Wiley and Sons, 2015.
- [8] Nazri F.M., Tan C.G. & Saruddin S.N.A., *Fragility Curves of Regular and Irregular Moment-Resisting Concrete and Steel Frames*, Int. Journal of Civil Engineering, **16**(8), pp. 917-927, 2018.
- [9] Ibrahim, Y.E., Shallan, O., El-Shihy, A. & Selim, M., Assessment of Seismic Damage of Multistory Structures Using Fragility Curves, Int. J. Engineering Research and Applications, 6(1), (Part 2), pp. 63-72, January 2016.
- [10] Hosseinpour, F. & Abdelnaby, A.E., *Fragility Curves for RC Frames Under Multiple Earthquakes*, Soil Dynamics and Earthquake Engineering, **98**, pp. 222-234, 2017.

- [11] Al Mamun, A. & Saatcioglu, M., Seismic Fragility Curves for Reinforced Concrete Frame Buildings in Canada Designed After 1985, Canadian Journal of Civil Engineering, 44(7), pp. 558-568, 2017.
- [12] Moon, D.S., Lee, Y.J. & Lee, S., Fragility Analysis of Space Reinforced Concrete Frame Structures with Structural Irregularity in Plan, ASCE J. Struct. Eng., 144(8), 2018.
- [13] Anvarsamarin, A., Rofooei, F.R. & Nekooei, M., Soil-Structure Interaction Effect on Fragility Curve of 3D Models of Concrete Moment-resisting Buildings, Hindawi, Shock and Vibration, pp. 1-13, 2018.
- [14] Mangkoesoebroto, S.P., Surahman, A., Batubara, S. & Irawan, P., *Investigation of Full-Scale Concrete Beam-Column Sub-Assemblies*, The Ninth East Asia-Pacific Conference on Structural Engineering and Construction, Bali-Indonesia, Dec. 2003.
- [15] FEMA, FEMA 356: Pre-standard and Commentary for the Seismic Rehabilitation of Buildings, Federal Emergency Management Agency, 2000.
- [16] Mangkoesoebroto, S.P. & Parithusta, R., Seismic Hazard Analysis of the Bandung Nuclear Reactor Site, PT Propenta Persisten Indonesia, 2005.
- [17] PEER, *Ground Motion Database*, Pacific Earthquake Engineering Research Center, 2018.
- [18] Ellingwood, B., Galambos, T.V., MacGregor, J.G. & Cornell, C.A., Development of a Probability Based Load Criterion for American National Standard A58. Building Code Requirements for Minimum Design Loads in Buildings and Other Structures, National Bureau of Standards Special Publication 577, US Department of Commerce, 1980.
- [19] Prayoga, M.H., Probabilities of Failure of Strong Column-Weak Beam Moment Resisting Reinforced Concrete Frame Structures Subjected to Seismic Ground Motions, Master Thesis, Faculty of Civil Engineering, Institute of Technology Bandung, Bandung, 2018.
- [20] ATC, ATC 40: Seismic Evaluation and Retrofit of Concrete Buildings, Applied Technology Council, 1996.
- [21] Mangkoesoebroto, S.P., Seismic Performance Chart for Simple Structures, Indonesia Center for Earthquake Engineering, 2007.
- [22] SEAOC, *Performance Based Seismic Engineering of Buildings*, Structural Engineering Association of California, 1995.
- [23] PEER, Modeling and Acceptance Criteria for Seismic Design and Analysis of Tall Buildings, Pacific Earthquake Engineering Research Center, 2010.
- [24] Haselton, C.B., Liel, A.B., Deierlein, G.G., Dean, B.S. & Chou, J.H., Seismic Collapse Safety of Reinforced Concrete Buildings. I: Assessment of Ductile Moment Frames, J. Struct. Eng., 137(4), pp. 481-491, 2011.